Rigorous Wilsonian renormalization group for impurity models with a spectral gap

Peter Zalom●*

Institute of Physics, Czech Academy of Sciences, Na Slovance 2, CZ-18200 Praha 8, Czech Republic

The Anderson impurity model (AIM) has long served as a cornerstone in the study of correlated electron systems. While numerical renormalization group (RG) offers great flexibility for metallic reservoirs, it becomes impossible in an unbiased way when a spectral gap Δ opens up in the tunneling density of states. The only known exception is provided by the superconducting bath. In this paper, we lift these limitations by developing a numerical RG procedure that employs a discretization of the gapped tunneling densities of states into patches that accumulate at the gap edges. This reveals an unusual double scaling, which is a shared behavior between the superconducting and the scalar gapped AIMs. Moreover, it requires a special iterative diagonalization procedure with an alternating scheme for discarding states only every second iteration. The discretization and the diagonalization scheme form together what we refer to as the log-gap numerical RG. It is successfully applied to the superconducting and to the scalar gapped AIM. Consequently, it reveals that both models belong to the same RG equivalence class, which manifests physically in common singlet-doublet quantum phase transitions accompanied by in-gap bound states of given parities. While superconducting AIM is mainly used for benchmarking the log-gap numerical RG, we also rigorously confirm the phenomenon of in-gap states escaping into the continuum. The gapped AIM is then tackled in an exact numerical RG approach and confirms quantitatively the assertions based on models with auxiliary metallic leads, but reveals that the other common approach used, for example, in the work of Moca and Roman [Phys. Rev. B **81**, 235106 (2010)] is of strictly approximate nature.

I. INTRODUCTION

The Anderson impurity model (AIM), proposed by Anderson in 1961 [1], has proven to be a fundamental framework for understanding a wide range of phenomena, including heavy fermions [2,3], quantum dots (QDs) in Coulomb blockade [4–7], or add atoms on normal surfaces [8,9]. It describes the behavior of localized electrons interacting with a continuum of itinerant states, encapsulating the complex interplay between localized and delocalized degrees of freedom, which is beyond the reach of perturbation theory.

The theoretical efforts it stimulated culminated by the computer-aided solution via the Wilsonian renormalization group (RG) [10–12], which is nowadays commonly known as the numerical RG (NRG). Quite recently, Wilsonian RG has also been applied to the AIM in the analytic framework of the functional RG techniques [13,14]. We also stress that several nonperturbative but approximate approaches are known to capture some of the aspects of the AIM [15–17], while at finite temperatures, the purely numeric approach via the quantum Monte Carlo (QMC) method is routinely used [18–20].

The main obstacle the RG targets specifically lies in the formation of mutually interconnected scales in the impurity systems. For metallic itinerant states, as the cascade approaches Fermi energy, it eventually gives rise to the Kondo effect. However, just by opening a spectral gap Δ, as present in superconducting [21–25] or semiconducting materials [22,26–29], we deprive the system of delocalized degrees of freedom at the Fermi energy, which severely impedes the energy cascade.

Intuitively, one expects an ordinary scaling of metallic AIM at temperatures much larger then Δ (all energy scales in this paper are measured in units of half-bandwidth B) to be present at least approximately. Formation of local magnetic moments and even Kondo-type screening is then anticipated for temperatures remaining much larger than the Kondo temperature T_K that corresponds to the $\Delta = 0$ case. Contrary, at temperatures much smaller than Δ no states are available to screen the impurity, and dramatic changes are expected. However, so far our understanding is complete only for the superconducting bath [30]. As we show here, this is also due to the fortunate nature of the one-lead problem, where the ordinary scaling of the AIM with constant metallic tunneling density of states (TDOS) is preserved.

For general gapped AIMs, no unbiased methods have so far reached the region of $\Delta \gg T$. While for QMC the restriction is fundamentally due to the computational resources, in the case of NRG the limitations are of methodological character as problems arise already in the first step when Wannier-type states are constructed for the delocalized electrons. Also, as shown here, the low-temperature scaling turns out to be unusual and requires crucial modifications to the diagonalization step of NRG.

*zalomp@fzu.cz

Up to date, general gapped AIMs are solved only indirectly or approximately with either a small but nonzero TDOS induced into the gap region by adding a weakly coupled metallic lead to the problem [21,22,26,31,32] or Wilson chains were constructed artificially from the corresponding models at $\Delta = 0$ [27,28,33]. While the first approach utilizes rigorous Wilsonian RG on a modified system, in the second approach, truncated Wilsonian chains of the AIM with constant metallic tunneling density of states (TDOS) are postulated to represent the gapped problem up to the energy scale of Δ. The two-scaled nature of the gapped problem is thus completely missed. Such results, as also clearly demonstrated in this paper, should therefore be understood as an approximate attempt. Nevertheless, qualitative conclusions from all currently available methods consensually confirm an unscreened impurity in the doublet ground state (GS) at $T = 0$ for a completely particle-hole symmetric scenario. Quantum phase transitions (QPTs) from a doublet to a singlet GS are observed upon further changing the orbital filling or particle-hole symmetry of the band [22,28].

While similar QPTs constitute basic phenomena in hosts of superconducting nature, the theoretic connection to the isolator and semiconductor problem was recognized only recently in Ref. [31], where the superconducting AIM (SC-AIM) was mapped onto a model with scalar gapped TDOS. Nevertheless, the two-scaled nature was not deciphered, as the resulting gapped AIM with specific TDOS was beyond the available NRG techniques and the system was augmented with a weakly coupled metallic lead. Additional studies of broad classes of gapped TDOS functions in Ref. [22] only reaffirmed these findings on a more general footing, but the study also suffered from implementing a weakly coupled metallic lead. Consequently, the existence of singlet-doublet QPTs could be so far asserted only indirectly, with the $T = 0$ behavior of truly gapped systems being only extrapolated.

In this paper, we therefore develop the NRG technique for general gapped AIMs with the afore-discussed two-scaled nature. We chose the gapped AIM with constant TDOS (defined in Sec. II A) and the SC-AIM (defined in Sec. II B) for the demonstrations. General restrictions on band discretizations are first given in Sec. III A with a general-purpose discretization proposed in Sec. III B. The resulting Wilson chains are then finally revealing a two-scaled behavior that is qualitatively the same for both models, despite additional divergences appearing in SC-AIM. The kept or discarded scheme of the standard NRG is then modified accordingly in Sec. IV to accommodate the scaling properties. The well-understood two-lead SC-AIM allows us then to validate the NRG technique in Sec. V A. Additionally, unique insights into the properties of subgap states are obtained here. We then proceed to the gapped AIM with piecewise constant but generally particle-hole asymmetric TDOS in Sec. V B and give an unbiased NRG solution to the problem. In Sec. V C, a detailed comparison with existing results on gapped AIM is performed. Here, we show that NRG methods with auxiliary metallic leads provided very good results, but techniques using redefined Wilson chains can only be used for qualitative assessment. In Sec. VI, the main results of the paper are subsequently briefly summarized.

II. THEORY

A. Gapped Anderson impurity model

For later convenience, we consider general AIM with two leads and a QD characterized by the Coulomb repulsion U and the level energy ε_d, which takes $-U/2$ at half-filled QD. However, we stress that the herein presented methods do not suffer from any limitations in this regard. The resulting Hamiltonian is then a sum of

$$H_d = \sum_\sigma \varepsilon_d d_\sigma^\dagger d_\sigma + U d_\uparrow^\dagger d_\uparrow d_\downarrow^\dagger d_\downarrow, \tag{1}$$

$$H_\alpha = \sum_{\mathbf{k}\sigma} \varepsilon_{\mathbf{k}\alpha} c_{\mathbf{k}\alpha\sigma}^\dagger c_{\mathbf{k}\alpha\sigma}, \tag{2}$$

$$H_{T,\alpha} = \sum_{\mathbf{k}\sigma} (V_{\mathbf{k}\alpha}^* c_{\mathbf{k}\alpha\sigma}^\dagger d_\sigma + V_{\mathbf{k}\alpha} d_\sigma^\dagger c_{\mathbf{k}\alpha\sigma}), \tag{3}$$

where $c_{\mathbf{k}\alpha\sigma}^\dagger$ ($c_{\mathbf{k}\alpha\sigma}$) creates (annihilates) an electron of spin $\sigma \in \{\uparrow\downarrow\}$, quasimomentum $\mathbf{k}$ in lead α which takes values L (left) or R (right lead). In analogy, $d_\sigma^\dagger$ (d_σ) creates (annihilates) a dot electron of spin σ, $\varepsilon_{\mathbf{k}\alpha}$ is an unspecified dispersion relation.

The QD hybridizes with the leads via $V_{\mathbf{k}\alpha}$, which we leave unspecified and instead prefer to extract the tunneling self-energy via

$$\Sigma(\omega^+) = \sum_{\alpha \in \{L,R\}\mathbf{k}} V_{\mathbf{k}\alpha}^* (\omega^+ - \varepsilon_{\mathbf{k}\alpha})^{-1} V_{\mathbf{k}\alpha} \tag{4}$$

and then demand its imaginary part (the tunneling TDOS) to a desired form. For constant but gapped TDOS with potentially particle-hole asymmetric band, we thus require

$$\text{Im}\Sigma(\omega^+) = \begin{cases} 0 & \text{for } |\omega| < \Delta, \\ [1 - \mathcal{A}\,\text{sgn}(\omega)]\Gamma_S & \text{for } |\omega| \geqslant \Delta, \end{cases} \tag{5}$$

where $\mathcal{A}$ governs the particle-hole asymmetry of the gapped band. In detail, for $\mathcal{A} = 0$ the TDOS remains symmetric as in Refs. [27,28] but for any $\mathcal{A} \neq 0$ different weights to the hole and electronic parts are ascribed.

B. SC-AIM in the scalar representation

An essential clue toward a unified theory of gapped AIMs was provided in Ref. [31] by the herein employed mapping procedure of SC-AIM. To briefly summarize the approach, we define SC-AIM with one QD and two superconducting leads. Its Hamiltonian is given as a sum of the QD Hamiltonian H_d according to (1), two tunneling Hamiltonians $H_{T,\alpha}$ in the form of (3), and two Hamiltonians $H_{\text{BCS},\alpha}$ describing the left ($\alpha = L$) and right ($\alpha = R$) leads via the Bardeen-Cooper-Schrieffer (BCS) theory which gives

$$H_{\text{BCS}} = \sum_{\mathbf{k}\alpha\sigma} \varepsilon_{\mathbf{k}} c_{\mathbf{k}\alpha\sigma}^\dagger c_{\mathbf{k}\alpha\sigma}$$
$$- \Delta \sum_{\mathbf{k}} (e^{i\varphi_\alpha} c_{\mathbf{k}\alpha\uparrow}^\dagger c_{-\mathbf{k}\alpha\downarrow}^\dagger + \text{H.c.}), \tag{6}$$

where Δ is the superconducting gap and φ_α are superconducting order parameters in the left and right leads. For this paper, we choose symmetric hybridizations Γ_L and Γ_R and the gauge

$\varphi_L = -\varphi_R = \varphi/2$ with φ being the phase difference across the SC-AIM. There is, however, no loss of generality due to the relation between symmetric and asymmetric coupling scenarios shown in Ref. [34]. It is now customary to employ the Nambu spinors

$$C_{\alpha \mathbf{k}}^\dagger = (c_{\alpha \mathbf{k} \uparrow}^\dagger, c_{\alpha -\mathbf{k} \downarrow}), \tag{7}$$

$$D^\dagger = (d_\uparrow^\dagger, d_\downarrow). \tag{8}$$

Under the standard BCS assumption of $\varepsilon_{\mathbf{k}\alpha} = \varepsilon_{-\mathbf{k}\alpha}$ and with a convenient choice of real tunnel couplings $V_{\alpha\mathbf{k}} = V_{\alpha\mathbf{k}}^* = V_{\alpha-\mathbf{k}}$, the Hamiltonians (2) and (3), apart from possible unimportant constant energy shifts, become

$$H_\alpha = \sum_{\mathbf{k}} C_{\alpha \mathbf{k}}^\dagger \mathbb{E}_{\alpha \mathbf{k}} C_{\alpha \mathbf{k}}, \tag{9}$$

$$H_{T,\alpha} = \sum_{\mathbf{k}} (D^\dagger \mathbb{V}_{\alpha \mathbf{k}} C_{\alpha \mathbf{k}} + C_{\alpha \mathbf{k}}^\dagger \mathbb{V}_{\alpha \mathbf{k}} D) \tag{10}$$

with

$$\mathbb{E}_{\alpha \mathbf{k}} = -\Delta_\alpha C_\alpha \sigma_x + \Delta_\alpha S_\alpha \sigma_y + \varepsilon_{\mathbf{k}\alpha} \sigma_z, \tag{11}$$

$$\mathbb{V}_{\alpha \mathbf{k}} = V_{\alpha \mathbf{k}} \sigma_z, \tag{12}$$

where σ_i, $i \in \{x, y, x\}$, are the Pauli matrices and $C_\alpha \equiv \cos \varphi_\alpha$, $S_\alpha \equiv \sin \varphi_\alpha$. The bold blackboard typeface distinguishes matrices from scalars. The corresponding TDOS is then given as

$$\mathbb{\Sigma}^D(\omega^+) = \sum_{\alpha \in \{L,R\} \mathbf{k}} \mathbb{V}_{\alpha \mathbf{k}} (\omega^+ \mathbb{1} - \mathbb{E}_{\alpha \mathbf{k}})^{-1} \mathbb{V}_{\alpha \mathbf{k}} \tag{13}$$

which yields

$$\mathbb{\Sigma}^D(\omega^+) = \Gamma_S \left[\omega \mathbb{1} + \Delta \cos \left(\frac{\varphi}{2} \right) \sigma_x \right] F(\omega^+) \tag{14}$$

with

$$F(\omega^+) \equiv \frac{1}{\pi} \int_{-B}^{B} \frac{d\varepsilon}{\omega^2 - \Delta^2 - \varepsilon^2 + i\eta \, \mathrm{sgn}(\omega)}$$
$$= \frac{1}{\pi \sqrt{(\omega + i\eta)^2 - \Delta^2}} \ln \frac{\sqrt{(\omega + i\eta)^2 - \Delta^2} + B}{\sqrt{(\omega + i\eta)^2 - \Delta^2} - B}. \tag{15}$$

Taking the $\eta \to 0$ limit, we arrive at

$$F(\omega^+) = \begin{cases} -\frac{2}{\pi \sqrt{\Delta^2 - \omega^2}} \arctan \left(\frac{B}{\sqrt{\Delta^2 - \omega^2}} \right) & \text{for } |\omega| < \Delta, \\ -\frac{i \, \mathrm{sgn}(\omega)}{\sqrt{\omega^2 - \Delta^2}} + \frac{\ln \left(\frac{B + \sqrt{\omega^2 - \Delta^2}}{B - \sqrt{\omega^2 - \Delta^2}} \right)}{\pi \sqrt{\omega^2 - \Delta^2}} & \text{for } \Delta < |\omega| < B. \end{cases} \tag{16}$$

The resulting $\mathbb{\Sigma}^D(\omega^+)$ has thus a nonzero imaginary part only for $|\Delta| < \omega$ while all effects of the finite-sized band appear in its real part. However, once the limit $B \to \infty$ is taken, the real part out of the gap vanishes too.

To bring the SC-AIM model into the form of general gapped AIM we perform the unitary transformation $\mathbb{T}$:

$$\mathbb{T} D \equiv W, \quad D^\dagger \mathbb{T}^\dagger \equiv W^\dagger, \tag{17}$$

where

$$\mathbb{T} = \frac{1}{\sqrt{2}} (\sigma_x - \sigma_z) \quad \text{and} \quad W^\dagger = (w_\uparrow w_\downarrow^\dagger). \tag{18}$$

The resulting TDOS in basis of W spinors is then

$$\mathbb{\Sigma}^W(\omega^+) = \Gamma_S \left[\omega - \Delta \cos \left(\frac{\varphi}{2} \right) \right] F(\omega^+). \tag{19}$$

Taking the imaginary part of (19) yields the TDOS for SC-AIM in the scalar representation with typical BCS divergences appearing at the edges while φ modulates the resulting particle-hole asymmetry in the basis of the w fields as shown in Fig. 1.

Finally, at half-filling the H_d Hamiltonian is form invariant against the transformation $\mathbb{T}$ and reads as

$$H_d = \sum_\sigma \varepsilon_d w_\sigma^\dagger w_\sigma + U w_\uparrow^\dagger w_\uparrow w_\downarrow^\dagger w_\downarrow. \tag{20}$$

III. NRG APPROACH FOR GAPPED TDOS FUNCTIONS

The here presented NRG approach generalizes the seminal work [35] to the gapped TDOS. We thus start in Sec. III A by generalizing the proof given in Ref. [35] to the gapped TDOS scenario. While the mathematical proof is relatively straightforward, it yields only limited specifications for the discretization procedure itself. Nevertheless, studying discretized self-energy as in Sec. III B allows for a preliminary justification to the here employed log-gap discretization. The resulting Wilson chains incorporate two separate scales in regimes of $T \gg \Delta$ and $T \ll \Delta$, respectively, which require significant modifications to the kept or discarded state scheme of the NRG diagonalizations as discussed in Sec. IV. We stress that z-averaging techniques can be potentially incorporated into the presented approach to improve, especially the spectral functions. However, in this paper, we focus on subgap spectroscopy and the validation of the developed NRG approach. We therefore set $z = 1$ throughout this work to streamline the presentation.

A. Gapped TDOS in the approach of Bulla

Let us assume that an impurity problem with gapped TDOS is present and its tunneling self-energy is given as

$$\Sigma(z) = \int_{I_\Delta} \sum_\mu d\omega \, V^2(\omega) \rho(\omega) G_\mu(\omega) \tag{21}$$

with $G_\mu(\omega)$ being the Green's function of the lead with a gapped DOS $\rho(\omega)$, while I_Δ denotes an integration interval running from $-B$ to B with a spectral gap of width 2Δ that is centered at the Fermi energy of 0. An example of such a self-energy is provided, for example, by Eq. (19). Our aim is now to construct a corresponding one-channel Hamiltonian

$$H - H_d = \int_{I_\Delta} \sum_\mu d\varepsilon \, g(\varepsilon) a_\mu^\dagger a_\mu$$
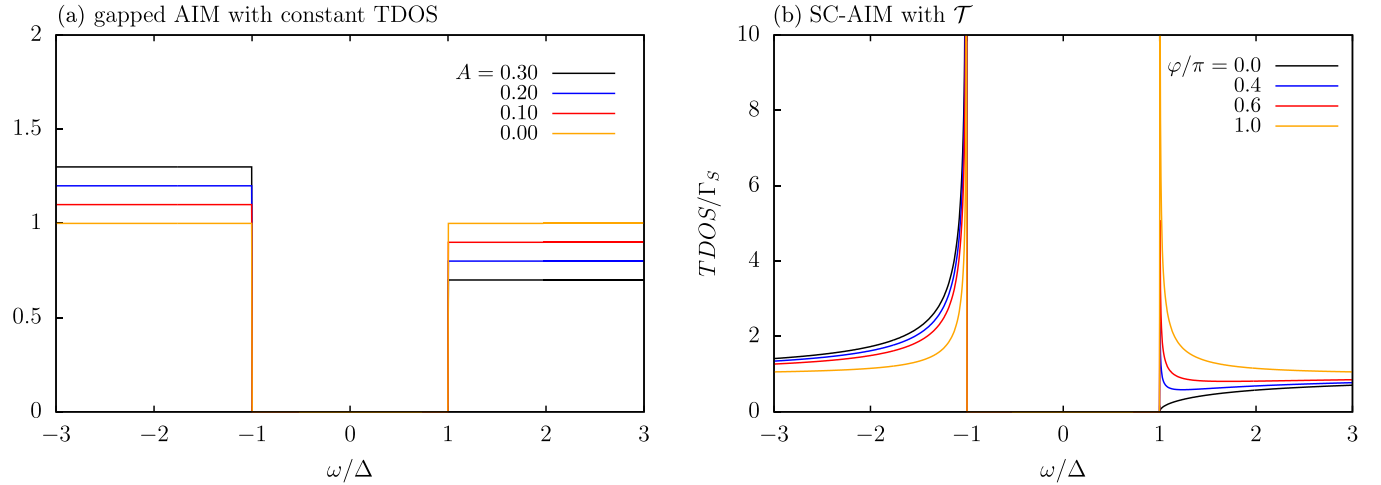$$+ \int_{I_\Delta} \sum_\mu d\varepsilon \, h(\varepsilon) d_\mu^\dagger a_\mu + \text{H.c.} \tag{22}$$

FIG. 1. (a) TDOS functions (5) of the gapped AIM with constant TDOS at various $\mathcal{A}$. The completely particle-hole symmetric case is obtained at $\mathcal{A} = 0$. (b) TDOS functions corresponding to SC-AIM in the scalar representation (19) for various phase differences φ. The completely particle-hole symmetric case is obtained at $\varphi = \pi$.

with $g(\varepsilon)$ and $h(\varepsilon)$ to be specified in such a way that the tunneling self-energy defined by (22) is identical to (21). We thus first change the integration variable from ε to g and solve for the tunneling self-energy of (22). We obtain

$$\Sigma(z) = \int_{I_\Delta} \sum_\mu dg \, h^2[\varepsilon(g)] \frac{d\varepsilon}{dg} G_\mu(g). \qquad (23)$$

Comparing (21) and (23) implies the following relation between $h(\varepsilon)$ and $g(\varepsilon)$:

$$V^2(x)\rho(x) = h^2[\varepsilon(x)] \frac{d\varepsilon}{dx}, \qquad (24)$$

which holds for every $x \in I_\Delta$ and has exactly the form known from Bulla's seminal work [35]. This is of crucial importance for gapped TDOS problems, as the discretization step can be performed without the introduction of any approximations. We may simply choose, for example, a piecewise constant $h(\varepsilon)$ on intervals $I_n^\pm$, where $+$ denotes intervals in positive and $-$ in negative frequency domain. To reconstruct the TDOS we can then transfer all required details onto $g(\varepsilon)$ via condition (24).

However, Eq. (23) gives us no prescription on how to choose the discretization intervals $I_n^\pm$. It just requires them to reside within the interval I_Δ. This leaves us with two main options, so n might be either a finite or infinite set of integer numbers. Since the tridiagonalization equations are of the same form as for the ordinary NRG, as applied for example to the AIM with metallic bath, a finite number of discretization intervals would leave us with a finite Wilson chain, which will inevitably have a smallest built-in energy scale. Moreover, the concept of approaching a low-temperature fixed point for Wilsonian RG iterations will make no sense at all.

To avoid such problems, one simply takes the iterative structure of the tridiagonalization equations into account by defining the initial discretization intervals $I_0^\pm$ that start at the band edges $\pm B$. As n is increased the intervals patch the remainder of I_Δ and get smaller towards the gap edges at

$\pm\Delta$. In formal agreement with Ref. [35], we then define the following quantities:

$$\xi_n^{+/-} = \frac{\int_{I_n^{+/-}} dx \, x \Gamma(x)}{\int_{I_n^{+/-}} dx \, \Gamma(x)}, \qquad (25)$$

$$(\gamma_n^{+/-})^2 = \int_{I_n^{+/-}} dx \, \Gamma(x), \qquad (26)$$

where $\Gamma(x)$ is the imaginary part of (21). These enter then subsequently the tridiagonalization equations (28)–(31) given in Ref. [36]. In detail, each interval I_n^+ (I_n^-) gives rise to operators $a_{n,\sigma,p}^\dagger$ ($b_{n,\sigma,p}^\dagger$). These are connected to a set of orthonormal functions indexed by $\pm$, n, and also p, where the last index takes all integer values. Inserting these into the corresponding Hamiltonians and taking piecewise constant approximation of the hybridization term in the energy representation allows only $p = 0$ components, so we can completely drop the p indices and obtain the corresponding discretized Hamiltonian as

$$H = H_{\mathrm{imp}} + \sum_{n,\sigma} (\xi_n^+ a_{n,\sigma}^\dagger a_{n,\sigma} + \xi_n^- b_{n,\sigma}^\dagger b_{n,\sigma})$$
$$+ \sum_n (\gamma_n^+ d^\dagger a_{n,\sigma} + \gamma_n^- d^\dagger b_{n,\sigma})$$
$$+ \sum_n (\gamma_n^+ a_{n,\sigma}^\dagger d + \gamma_n^- b_{n,\sigma}^\dagger d). \qquad (27)$$

B. Log-gap discretization for gapped AIMs

To guide us in the choice of the precise form of the discretization intervals $I_n^\pm$ we now solve for the discretized tunneling self-energy $\Sigma_{\mathrm{disc}}(z)$ of (27). It reads as

$$\Sigma_{\mathrm{disc}}(z) = \sum_n \frac{-(\gamma_n^+)^2}{\xi_n^+ - z} + \frac{(\gamma_n^-)^2}{-\xi_n^- + z}. \qquad (28)$$

The two branch cuts of the continuous $\Sigma(z)$ that follow the real axis and terminate at $\pm\Delta$ have thus been replaced by simple isolated poles at positions $\xi_n^+ > 0$ and $\xi_n^- < 0$. The coefficients (25) have thus a straightforward meaning of the

positions of the poles, while (26) defines the corresponding weights in the discretized TDOS.

Analogous results are present also in other commonly used approaches to NRG. For example, in AIM with a logarithmic discretized metallic reservoir, the continuous self-energy with branch cut over the entire real axis gives rise to simple poles that accumulate logarithmically around the Fermi energy. From the perspective of gapped systems, they accumulate exactly where the two branch cuts over the positive and negative parts of the real axis merge as $\Delta = 0$. Similar pattern is also observed for the superconducting bath, which is the only system with a spectral gap that is currently rigorously treated by NRG and thus closest to the problem advanced here. Once again, using standard two-channel NRG techniques for SC-AIM the discretized tunneling self-energy $\Sigma_{\mathrm{disc}}(z)$ is obtained in the form of (28) with simple poles emerging along the two branch cuts. Significantly, they are known to accumulate logarithmically at the terminal points $z = \pm\Delta$ of the branch cuts.

Our aim now is therefore to construct a discretization that is not only in line with the requirements of the previous section but reproduces additionally the logarithmic accumulation of simple poles in the corresponding tunneling self-energy $\Sigma_{\mathrm{disc}}(z)$ at $z = \pm\Delta$ where the branch cuts of the continuous self-energy terminate. To this end we define the intervals $I_n^{\pm}$ via their end points $x_n^{\pm}$ as

$$x_n^{\pm} = \pm[\Delta + (1 - \Delta)\Lambda^{-n}], \tag{29}$$

where Λ is the usual discretization parameter with intervals $I_n^{\pm}$ obviously aggregating at the gap edges in a logarithmic way (bandwidth set as $2B \equiv 2$). Consequently, we refer to (29) as the log-gap discretization. We stress that it was already considered in Ref. [37]. However, the scaling properties of the resulting Wilson chains have been completely missed and the employed standard kept or discarded scheme may have resulted in ill-converging solutions at low temperatures, which the authors did not report in the paper. As shown in the next section, further modifications to the NRG approach are required to resolve this problem.

Let us now calculate the pole structure of the discretized self-energy. First, we consider the gapped Anderson model with TDOS (5). We note that the discretized self-energy becomes of form (28) with poles $\xi_n^{+/-}$ and weights $\gamma_n^{+/-}$ obeying

$$\xi_n^{+/-} = \pm\left[\Delta + \frac{(1 - \Delta)(1 + \Lambda)}{2}\Lambda^{-1-n}\right], \tag{30}$$

$$(\gamma_n^{+/-})^2 = (1 \pm \mathcal{A})(1 - \Delta)(\Lambda - 1)\Lambda^{-1-n}. \tag{31}$$

Setting $\Delta = \mathcal{A} = 0$, one recovers the standard case of the AIM with constant metallic TDOS, where poles approach the gap edges in a logarithmic fashion. The same holds true also for $\Delta \neq 0$ at arbitrary $\mathcal{A}$, only this time the poles are logarithmically approaching the gap edges, as in the standard NRG approach to SC-AIM. The log-gap discretization is thus increasingly sensitive to the states that get closer to the Fermi energy, albeit due to the presence of the gap, it is never reached. Notably, poles (30) are placed symmetrically around the Fermi energy, regardless of the values of $\mathcal{A}$ and/or Δ. Consequently, the particle-hole asymmetry is completely encoded only by the weights $\gamma_n^{+/-}$.

Since the constant gapped TDOS is structureless at the gap edges, let us also corroborate the SC-AIM case in its scalar representation as shown in Fig. 1. The BCS-like divergences on the gap edges and a complicated particle-hole asymmetry of (19) lead to the following expression:

$$\xi_n^{+/-} = \pm[\Delta + f^{\pm}(\varphi, \Delta, \Lambda)\Lambda^{-1-n}], \tag{32}$$

where the prefactors $f^{\pm}(\varphi, \Delta, \Lambda)$ are functions of Δ and Λ and are generally not particle-hole symmetric, i.e., $f^+(\varphi, \Delta, \Lambda) \neq f^-(\varphi, \Delta, \Lambda)$, unless $\varphi = \pi$. Consequently, the overall particle-hole asymmetry of (19) is distributed over poles and weights of the discretized self-energy, causing an effect that needs to be addressed later. Nevertheless, the logarithmic behavior toward the terminal points of the branch cuts is still preserved, but compared to the standard SC-AIM solution, the poles are not distributed in a particle-hole symmetric fashion, which is an effect that needs to be considered later as a potential source of differences.

Next, we will feed the poles and weights into the tridiagonalization equations of Ref. [36] to obtain the corresponding Wilson chains. Due to the corroborated differences to the only known standard NRG solution, we chose the SC-AIM case for these demonstrations. We select $\Gamma = \Delta$, $U = 3\Delta$, $\varepsilon_d = -U/2$ and vary φ. The resulting parameters of Wilson chains for selected values of φ are then shown in the first row of Figs. 2(a)–2(d), while the second and third rows demonstrate high- and low-temperature scalings of the hoppings, respectively.

As shown in the first row of Figs. 2(a)–2(d), at large n even hoppings become approximately $\Delta\sin\varphi$, while odd hoppings become exponentially suppressed. To decipher the various scalings present in the system, let us look at the second and third rows of Figs. 2(a)–2(d). Obviously, there is always an initial stage where hoppings scale in an usual $\Lambda^{-n/2}$ way, which however survives down to $n \to \infty$ only for $\varphi = 0$. Otherwise, the scaling is interrupted by a crossover region, and only odd hoppings scale exponentially with Λ^{-n} law.

The behavior of the onsite energies ϵ_n, on the other hand, is more straightforward as they vary between the approximate values of $\pm\Delta\cos(\varphi)$. The alternating pattern holds approximately for all model parameters when the log-gap NRG approach is applied with only particle-hole symmetric TDOS leading to the vanishing of all onsite energies.

While the presented cases were calculated for SC-AIM, we stress that the alternating feature of the onsite energies and the two-scaled nature of hoppings are also observed for the gapped AIM model with constant TDOS function. However, here, the second stage of scaling involves odd hoppings that follow the $\Lambda^{-n/2}$ law. So clearly, the presence of the additional BCS-like divergencies in the TDOS of the SC-AIM case modifies the power law of the odd hoppings in the low-temperature regime.

IV. ITERATIVE NRG DIAGONALIZATION OF TWO-SCALED WILSON CHAINS

The observed two-scaled nature of the hoppings is an essential feature that needs to be adequately considered during the iterative NRG diagonalization. To begin with, let us however first discuss the special case of $\varphi = 0$ which exhibits
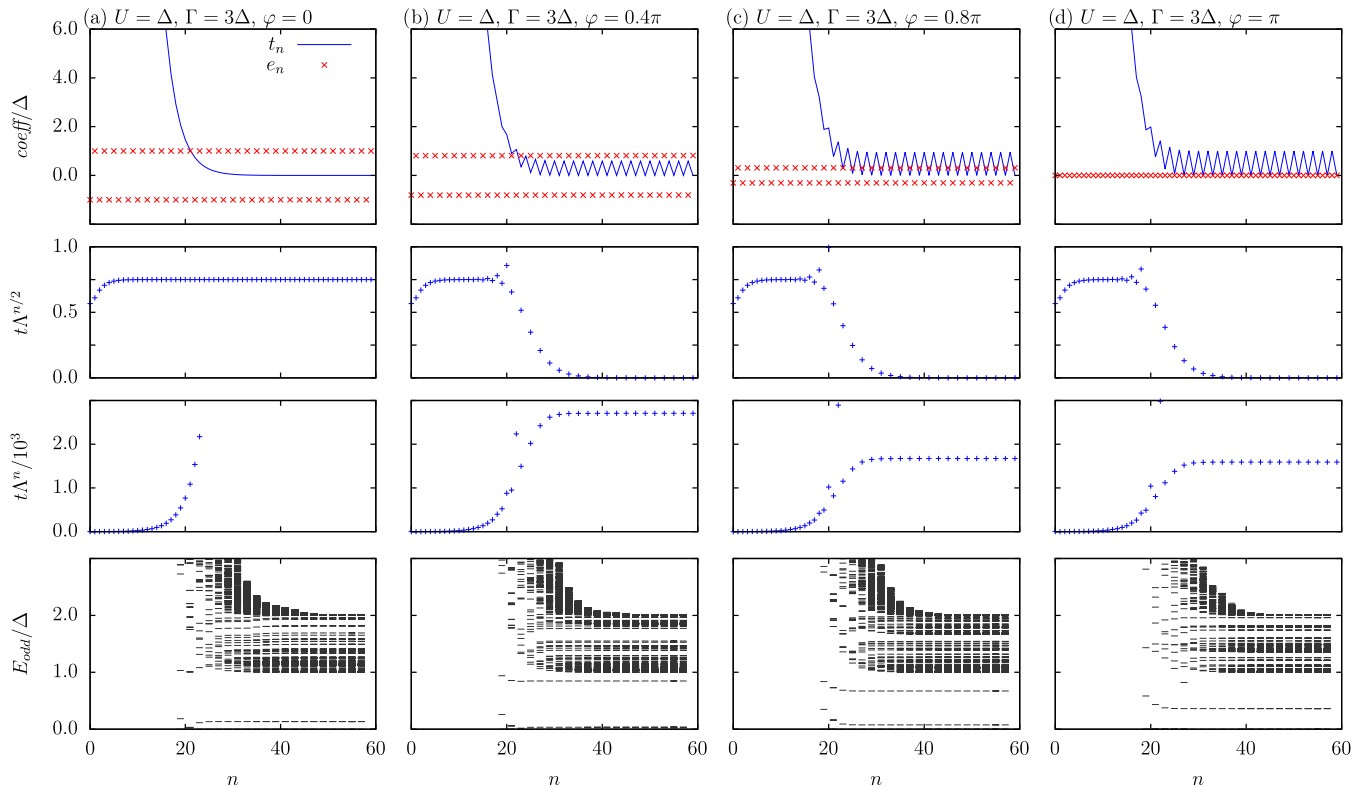
FIG. 2. (a)–(d) Hoppings t_n (solid blue line), onsite energies ϵ_n (red crosses), and the corresponding energy eigenvalues (gray lines) of the Wilson chain of length n calculated via the log-gap approach for SC-AIM with $U = 3\Delta$ and $\Gamma = \Delta$ at several phase differences φ. First row shows unrescaled values of Wilson chain parameters. The onsite energies ϵ_n are alternating in the sign, but their absolute value is approximately constant. However, hoppings t_n follow two successive scalings. The first one with $t_n \sim \Lambda^{-n/2}$ is shown in the second row and applies to high temperatures ($T \gg \Delta$). Upon decreasing the phase bias toward $\varphi = 0$ the region of high-temperature scaling increases until it dominates the entire temperature range for $\varphi = 0$. The third row shows then the low-temperature ($T \ll \Delta$) scaling of hoppings obeying $t_n \sim \Lambda^{-n}$, which sets in after the short crossover region of approximately 10 NRG iterations. The last row shows eigenenergies obtained using the log-gap NRG approach with a diagonalization scheme according to Sec. IV. Correct energy scale separation is observed.

only the ordinary $\Lambda^{-n/2}$ scaling for all hoppings and was first described in the seminal papers on NRG [10–12]. Iterative addition of the sites of the Wilson chains leads to an exponential increase of the total Hilbert space, which is dealt with by a truncation strategy as illustrated in Fig. 3(a). Thus, already after a few NRG iterations, high-energy states (multiplets) are being discarded systematically, with a more or less constant number kept until the algorithm is stopped.

Such a diagonalization procedure works only in conjunction with the $\Lambda^{-n/2}$ scaling of all hoppings and ensures energy scale separation (high- and low-eigenenergy states do not mix as the chain grows). While originally established for impurities in metallic baths, the same scaling and consequently energy separation emerge also for one-lead SC-AIM problems [38]. Quite surprisingly, and without an apparent justification, it was also established for the two-lead SC-AIM, where the addition of complex phases mixes both leads together [23].

In our case, such mixing is also observed once $\varphi \neq 0$ and leads to the second stage of scaling, where even hoppings approach $\Delta \cos\varphi$ and odd hopping scale as Λ^{-n}. In this second stage, we can thus naturally reinterpret the Wilson chain as being composed of serial double QDs interconnected by exponentially decreasing hopping. If the Hilbert space is never truncated after the odd site is added, splittings of eigenenergies by factor proportional to Λ^{-n} have to

occur at even iterations, and energy scale separation can be exploited.

As demonstrated graphically in Fig. 3(b), such a kept or discarded strategy is perfectly tailored for the low-energy scaling, but it would be difficult to be turned on only after one emerges from the initial scaling. Fortunately, when applied also to the high-temperature portion of the Wilson chain, the kept or discarded strategy just keeps superfluous high-energy states (multiplets) every odd iteration. At even iterations, they give rise to states that are immediately discarded, so in principle, the kept or discarded strategy is just inefficient in the $\Lambda^{-n/2}$ scaling sector but does not break the energy scale separation as demonstrated in the fourth row of Fig. 2(a) by the $\varphi = 0$ case where second-stage scaling is not present at all. Here, eigenenergies at odd NRG iterations $E_{\rm odd}$ (no rescaling applied) clearly converge as n is increased up to 60. Modifications to the kept or discarded strategy in the low-temperature sector are thus not necessary and can be potentially reverted to speed up the numerics, which however requires careful investigations. Such refinements are left for future developments.

For all other values of φ the second-stage scaling occurs after a crossover region, but as shown in the fourth row of Figs. 2(b)–2(d) the kept or discarded strategy indeed ensures energy scale separation. We also stress that at every
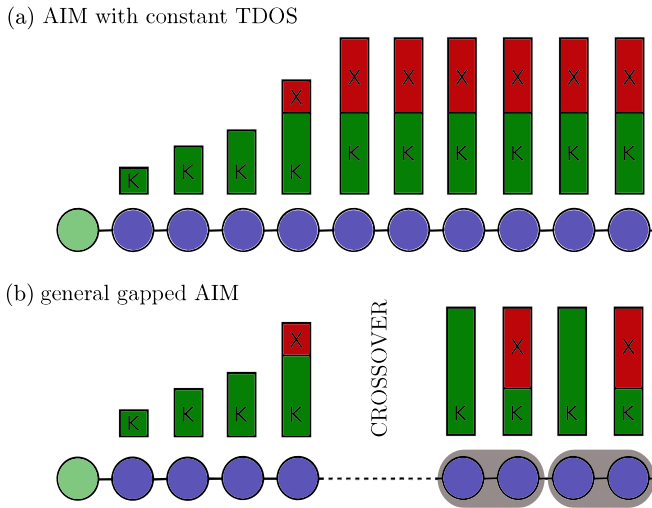
(a) AIM with constant TDOS

(b) general gapped AIM

FIG. 3. (a) An illustration of the outcome of the ordinary strategy to keep (green, letter K) or discard (red, letter X) states (or multiplets) during iterative NRG diagonalization of AIM with metallic TDOS. After few initial iterations, a maximum number of kept states is quickly reached. (b) The Wilson chain of a general gapped AIM incorporates an initial scaling of odd and even hoppings as $t_n \sim \Lambda^{-n/2}$ which undergoes a smooth crossover into the second-stage scaling, where odd hoppings scale as Λ^{-n} and the even ones reach a constant value. To ensure energy scale separation, it is thus necessary to keep all states at odd NRG iterations. Such an alternating kept or discarded scheme reinterprets the Wilson chain into a tight-binding Hamiltonian of noninteracting serial double QDs.

NRG iteration, new low-energy states resurface around the gap edge (not including the subgap states) and get exponentially close to the region right above the gap edge as n is increased. Their appearance does not, however, alter the other higher-lying eigenvalues, which are already converged. This is, of course, a feature well known also from the standard NRG solution of SC-AIM as discussed in the Appendix of Ref. [38].

The strategy of keeping or discarding states comes with the price of increased CPU and memory requirements over the traditional scheme of Fig. 3(a) since the intermediate Hilbert space used for matrix diagonalizations grows by factor of up to 16, which thus resembles the ordinary two-channel NRG calculations. However, in the scalar basis used here, charge and pseudospin quantum numbers label the states (multiplets), and the increased symmetry is crucial for speeding up the diagonalizations when the log-gap NRG approach is employed. Consequently, the here proposed NRG scheme for SC-AIM remains feasible at any modern desktop also when $\varepsilon \neq -U/2$ and even in the presence of nonzero magnetic field, while the standard two-channel NRG solution reaches limits of its practical feasibility.

Apparently, the same kept or discarded strategy is also required for the AIM with constant but gapped TDOS, albeit the odd hoppings of the second-stage scaling follow the $\Lambda^{-n/2}$ law. Still, the even hoppings alternate between positive and negative values. Consequently, the low-temperature portion of the Wilson chain has once again the character of a tight-binding chain composed of serial double QDs connected by exponentially decreasing hoppings. The application of the log-gap NRG with the modified kept or discarded strategy then finally also confirms functioning energy scale separation.

The kept or discarded scheme of Fig. 3(b) is crucial for performing unbiased Wilsonian RG calculations for the here discussed models. We would like to briefly explore the outcome when an ordinary kept or discarded scheme according to Fig. 3(a) is employed even for Wilson chains of the two-scaled nature. The energy scale separation is then, of course, not ensured, and the eigenspectrum of energies becomes corrupted for $\varphi \neq 0$ or $\varphi \neq \pi$ as demonstrated in Appendix A. Nevertheless, problems occur initially only in its high-energy part, and the subgap spectrum remains largely intact, so intermediate NRG iterations can be used to determine subgap properties with only a few percent of relative error when compared to the rigorous Wilsonian approach developed here. We will call this approach the approximate log-gap NRG, although we stress that it is actually a misnomer as energy scale separation is broken. It should thus strictly be used only for fast scanning and, at least, a portion of the data should always be validated against rigorous methods. Additionally, supragap spectral functions or thermodynamic properties depend upon high-energy states and will thus be susceptible to much larger systematic errors. In the main part of this paper, we will therefore use only the here developed rigorous log-gap NRG and will briefly discuss the veracity and possibilities of its fast but approximate version in Appendix A.

V. RESULTS

A. SC-AIM

In the previous sections, a rigorous Wilsonian NRG scheme has been developed to tackle arbitrary problems with QD immersed in a gapped TDOS. Before solving the gapped Anderson model, as an example, we first validate the log-gap NRG against the well-established two-channel standard solution of SC-AIM by using its scalar representation derived in Ref. [31]. We will also demonstrate its effectivity in regard to the CPU time by obtaining the full phase diagram and will exploit the quantum numbers for tracking of in-gap excitations as they leave into the continuum, which was currently speculated upon in Ref. [40].

Starting by obtaining the complete phase diagram for SC-AIM with QD at half-filling in Fig. 4, we notice that the resulting singlet-doublet QPT lines divide the $\Gamma/\Delta-U\Delta$ plane into the upper-doublet GS portion and the lower-singlet GS part. Four selected values of φ are shown with $\varphi = \pi$ leading to the exclusive doublet GS phase for all parameters as long as $\varepsilon_d = -U/2$. Due to the employed symmetries in the log-gap NRG solution of SC-AIM, the calculations come only at a fraction of the CPU time required by the ordinary NRG and are feasible on any modern desktop. We have thus precalculated the data in Fig. 4 via the log-gap approach and used these as an ansatz for the standard NRG calculations (points).

The resulting parity transition lines obtained using the log-gap NRG approach with $\Lambda = 2$ (solid lines) are then compared to the standard two-channel NRG calculations at $\Lambda = 4$ (points). While only a small and steady difference
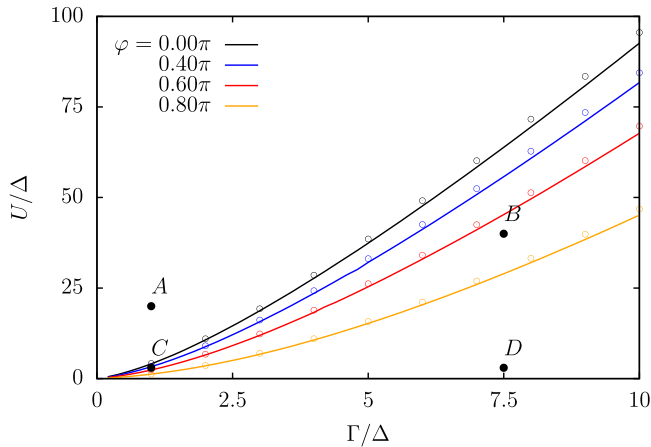
FIG. 4. The phase transition lines of SC-AIM calculated via the log-gap NRG (solid lines) and the standard two-channel NRG approach (points) at four different values of φ. QD is set to half-filling via $\varepsilon_d = -U/2$. The doublet (singlet) phase is realized above (below) the lines. The difference between both methods is $\approx 3\%$ and steady for all shown data points. The comparison for the phase-dependent position of ABS states is undertaken for the four selected cases A, B, C, and D in Fig. 5.

of $\approx 3\%$ between both methods is observed, we select four cases A, B, C, and D at various ratios of U/Γ for a detailed study. The QD is still held at half-filling via $\varepsilon_d = -U/2$. The resulting subgap spectroscopy including one- and two-particle excitations is then presented in Fig. 5. Once again the log-gap NRG approach with $\Lambda = 2$ (solid and dashed lines for one- and two-particle excitations, respectively) and the standard two-channel NRG with $\Lambda = 4$ (open circles) are generally in very good agreement, but the difference systematically grows as φ is decreased. This hints toward an increasing importance of the asymmetric pole structure of the self-energy due to the log-gap discretization, while the effect of different Λ appears less significant.

In case A, the ratio $U/\Gamma = 20$ drives the system into the doublet GS phase for all possible values of φ. An opposite scenario at small ratio of U/Γ, case D, is then conversely marked by singlet GS phase dominating almost the entire phase evolution. The doublet GS phase is, however, always present, albeit only in a small region around $\varphi \approx \pi$ due to the phenomenon of the doublet chimney as explained in Ref. [39]. Cases B and C have, on the other hand, moderate ratios U/Γ, which results in comparably similar phase regions of singlet and doublet GS phases.

Additionally, the developed NRG technique assigns charge and pseudospin numbers to the NRG eigenstates and allows direct tracking of the in-gap excitations as they cross into the continuum region in cases B, C, and D. Only case A is an exception since the continuous part of the spectrum and the state corresponding to the excitation of interest share similar quantum numbers. The directly observed values have then been used to cross identify the most likely candidates from the standard two-channel NRG calculations. Our observations are in good accord with the indirect observations in Ref. [40].

B. Gapped AIM with constant TDOS

The successful comparison between the log-gap and the standard NRG approach from the previous section enables us to move forward with addressing the gapped AIM problem, maintaining a constant TDOS, which is notably simpler compared to the TDOS of the SC-AIM. Providing a comprehensive and unbiased NRG solution for the gapped AIM problem with constant TDOS allows us present the observed physical phenomena and highlight their connection to the shared RG equivalence class with the SC-AIM. Our primary focus will be on examining the impact of particle-hole asymmetry, which arises both from the band (parameter $\mathcal{A}$) and the filling of the orbital (determined by the level energy ε_d). It is worth noting that in this section, all data will be cross verified against the NRG method employing auxiliary metallic leads, which it replicates convincingly. However, a more detailed discussion on this topic will be deferred to a dedicated section in Sec. V C.

For now, let us start with the phase diagram of the problem with QD at half-filling as shown in Fig. 6. Using the log-gap discretization, the resulting Wilson chains for gapped AIMs are of one-channel nature and can be diagonalized in a standard iterative approach of NRG. The resulting GS parity can be read off directly, unlike in NRG methods with auxiliary metallic leads. The hypothesis about the GS and in-gap parities of Ref. [22] are nevertheless finally directly confirmed. Consequently, GS transition lines divide the $U/\Delta - \Gamma/\Delta$ plane into an upper-doublet and a lower-singlet portion. Overall, the similarity to the phase diagram of SC-AIM in Fig. 4 is exemplary.

The particle-hole asymmetry $\mathcal{A}$ of the gapped band plays an analogous role as φ in SC-AIM in its scalar representation. In detail, $\mathcal{A} = 0$ and $\varphi = \pi$ correspond to each other and represent the particle-hole symmetric choices for the corresponding models. Consequently, at $\mathcal{A} = 0$ the whole $U/\Delta - \Gamma/\Delta$ plane supports only the doublet GS, giving rise to the phenomenon of doublet chimney as discussed in Ref. [39] specifically for SC-AIM. Nevertheless, inducing even a small particle-hole asymmetry $\mathcal{A}$ causes a QPT into the singlet GS at large hybridizations Γ/Δ. The larger the particle-hole asymmetry $\mathcal{A}$ becomes, the more extended the singlet phase space becomes. All of these findings point to a deeper connection between SC-AIM and other gapped AIMs as hypothesized already in Ref. [22]. In the present approach, the connection is already evident after the discretization step is performed, as the two-scaled Wilson chain emerges for both models.

To further deepen these findings, we select four cases A, B, C, and D with exactly the same U/Δ and Γ/Δ as in the SC-AIM case. We then calculate the evolution of the in-gap excitations with respect to the particle-hole asymmetry parameter $\mathcal{A}$ as shown in Fig. 7 and use solid (dashed) lines to track the one-particle (two-particle) excitations. We stress that unlike in SC-AIM, in-gap excitations do not come in pairs except of $\mathcal{A} = 0$, but this is a trivial consequence of gapped AIM being directly defined in the basis of (generally) particle-hole asymmetric fermions. Anyway, to make the correspondence to the SC-AIM problem more obvious, we also add excitations that appear for the model upon $\mathcal{A} \to -\mathcal{A}$, but we stress that they never appear simultaneously.
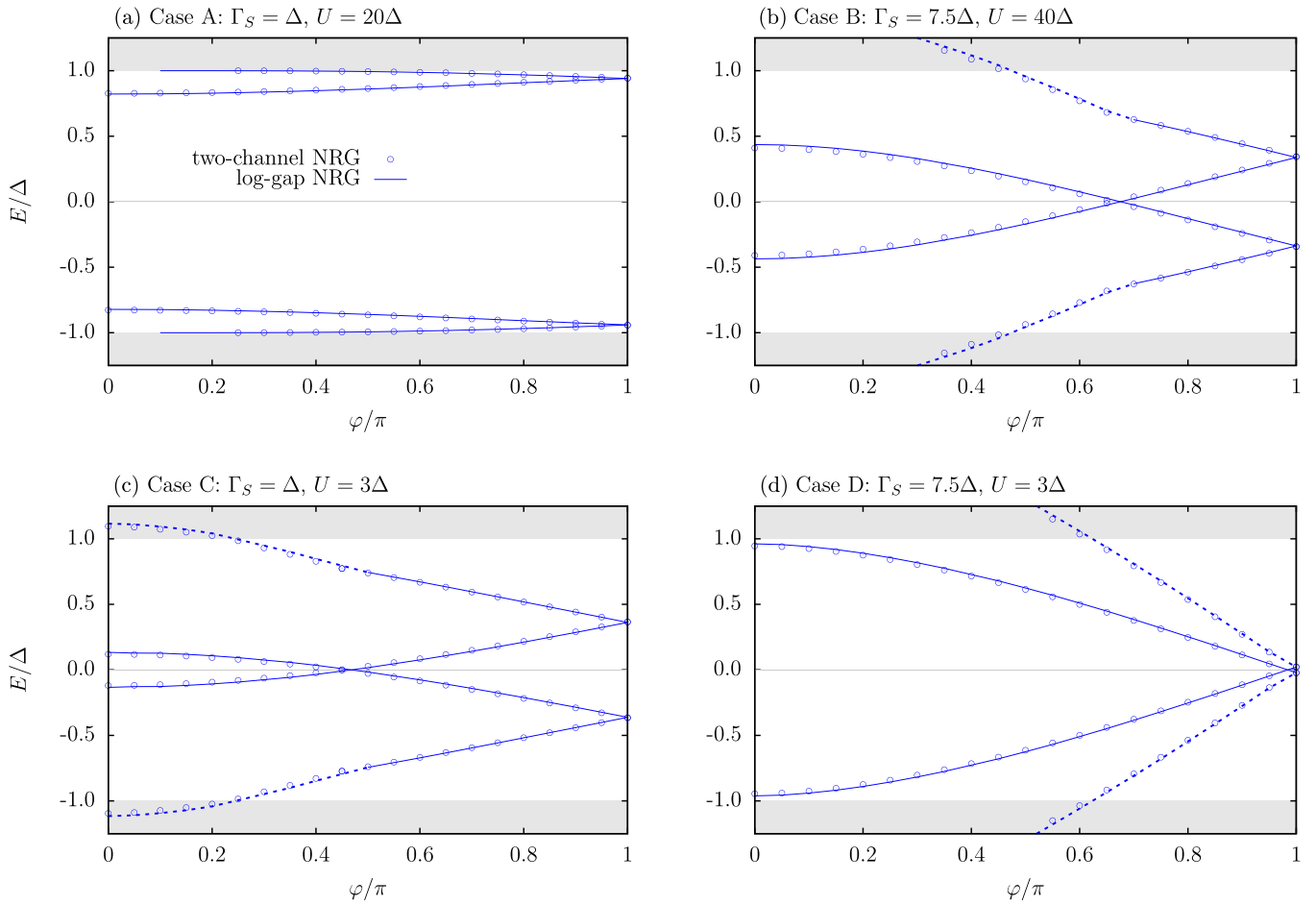
FIG. 5. (a)–(d) φ-dependent behavior of subgap excitations for four selected cases A, B, C, and D of SC-AIM with parameters according to Fig. 4. Note that QD is at half-filling due to $\varepsilon_d = -U/2$. Solid lines represent the ABS states, while dashed lines show the two-particle excitations calculated by the log-gap NRG approach at $\Lambda = 2$. The reference data were calculated using the two-channel NRG with $\Lambda = 4$ (open circles). The agreement is overall very good, but a systematic tendency of increased differences occurs as φ tends towards 0. The escape of subgap states into the continuum portion of the spectrum was rigorously verified in cases B, C, and D via the log-gap NRG approach, and only subsequently could the corresponding states from the two-channel NRG could be identified.

In detail, the large Coulomb interaction in case A expels the singlet in-gap states to the edge of the subgap region and ensures doublet GS for all values of $\mathcal{A}$. At $\mathcal{A} = 0$, the underlying symmetry causes both singlet excited states to overlap, which appears then as two symmetrically placed one-particle excitations in the subgap spectral function. At $\mathcal{A} \neq 0$, one of these singlets is pinned to the gap edge and starts moving closer to the Fermi energy only as $\mathcal{A} \approx 0.5$. The other singlet crosses then into the continuum part of the spectrum. The only difference to the SC-AIM case lies thus in a different curvature of the observed trajectories, which is of quantitative nature and clearly depends on the shape of the TDOS. The case D shows then in analogy an contrasting outcome to case A. Due to the large hybridization Γ, already a very small particle-hole asymmetry of $\mathcal{A} \approx 0.01$ suffices to induce a doublet-singlet QPT. Consequently, the singlet phase dominates the in-gap states.

The outcome in cases B and C is once again in close analogy to the SC-AIM results with the initial doublet GS being present up to moderate values of $\mathcal{A} \approx 0.25$. The first excited state at $\mathcal{A} = 0$ is of doublet nature and appears in hole

as well as particle part of the spectral function. Increasing then $\mathcal{A}$ causes both in-gap peaks of the spectral function to move in the same direction towards the gap edge. Together with their symmetric counterparts (thin gray lines), which physically appear together only in SC-AIM, we observe a typical W-shaped pattern. Once again, up to the missing symmetrization both models behave qualitatively in an analogous way. These findings are thus consistent with the hypothesis of Ref. [22], where both models are stipulated to belong to the same RG universality class.

Finally, we can investigate how the filling of the QD, and the particle-hole asymmetry it induces, affect the system. Within the framework of log-gap NRG, in situations where the band exhibits particle-hole symmetry (e.g., $\mathcal{A} = 0$), the onsite energies of the corresponding Wilson chain, derived from log-gap discretization, effectively vanish, leaving us with chain exhibiting a single scaling law as hoppings become $t_n \propto \Lambda^{-n/2}$ (n is the iteration number). Attaching a QD with arbitrary ε at the beginning of the Wilson chain has absolutely no influence on its parameters, instead, only the RG flow is altered through the impact of the initial iteration. As a result,
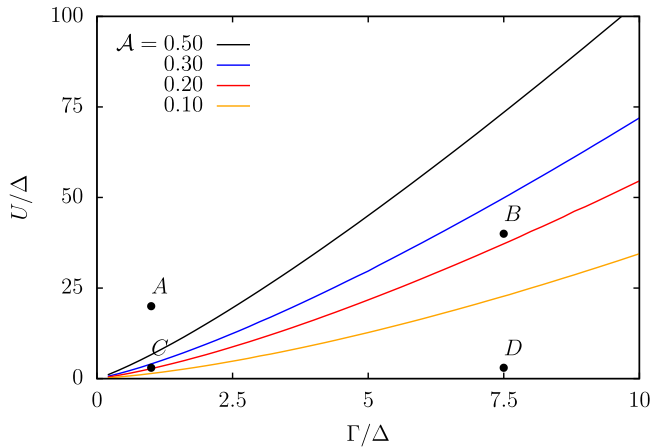
FIG. 6. Phase boundaries between the singlet and doublet GS for four selected values of particle-hole asymmetry parameter $\mathcal{A}$ of the gapped AIM with constant TDOS. The case of $\mathcal{A} = 0$ results in purely doublet GS and is thus not shown. Nevertheless, the phase diagram clearly indicates that even a proportionally small amount of particle-hole asymmetry is enough to cause a transition into a singlet phase at large hybridizations Γ. The phase diagram also clearly indicates relationship to the SC-AIM shown in Fig. 4.

the alternating kept or discarded diagonalization scheme, necessary for $\mathcal{A} \neq 0$ scenarios, becomes superfluous.

However, it is our intention to document that log-gap NRG, even with the alternating kept or discarded scheme still applied, works seamlessly. To illustrate this, we have once again chosen cases A, B, C, and D of Fig. 6, set $\mathcal{A} = 0$, and varied ε_d/U accordingly to obtain Fig. 8. The observed evolution of subgap spectrum qualitatively mirrors the effects induced by particle-hole asymmetric bands. As a measure of the induced particle-hole asymmetry, we utilize $\delta = \varepsilon_d + U/2$, which places the QD at half-filling when $\delta = 0$.

In more detail, for $\mathcal{A} = \delta = 0$ the system consistently attains a doublet GS with subsequent excitation levels taking on singlet characteristics. We observe a symmetric pair of in-gap states in all cases. Albeit, due to the extreme values of ratio U/Γ, cases A and D expel the in-gap states against the gap edge or the Fermi level, respectively. In case A, a relatively significant rate of particle-hole asymmetry, e.g., $\delta/U \approx 0.5$, is required to drive the in-gap state close to the Fermi energy, where a doublet-singlet QPT can be enforced. Contrary to this, in case D the in-gap state is already near to the Fermi energy, necessitating a much smaller particle-hole asymmetry, e.g., $\delta/U \approx 0.2$, to induce the QPT.

For cases B and C, where the ratio of U/Γ is more modest, the in-gap states initially reside in the middle of the gap. As δ increases, both states gradually move toward the same gap edge. Eventually, as the induced particle-hole asymmetry rises, one of the states crosses the Fermi energy, marking a doublet-singlet QPT. Remarkably, we once again observe two-particle excitations in the subgap region, eventually escaping into the continuum. In all of the cases, the data have been compared with the NRG method that employs a weakly coupled metallic lead, and the agreement is convincing. Notably, the log-gap NRG allows for tracking all in-gap peaks across the entire parametric range, whereas the second method

encounters difficulties of numeric nature each time the in-gap peaks move close to the gap edge or the the Fermi energy.

From a physical standpoint, it is intriguing to note that particle-hole asymmetry manifests qualitatively similar effects in the subgap energy range. On the level of Wilson chains, this becomes transparent starting from the initial NRG iterations, as energy levels acquire additional splittings, which happen irrespective of the origin of the particle-hole asymmetry. However, for the band-induced effect, the splittings become comparable with the eigenvalues only as the low temperature is approached, while for $\delta \neq 0$ such accumulations are not observed.

It is worth emphasizing that log-gap NRG allows us to investigate both effects concurrently, which is of high practical value. Furthermore, log-gap NRG proves versatile enough to handle scenarios where the Fermi energy does not lie in the middle of the energy gap [41]. In this case, a simple modification to the discretization procedure is required. Consequently, the electronic and hole parts of TDOS are to be handled individually by log-gap discretization, with each providing its own gap parameter measured against the Fermi energy. The resulting Wilson chains then exhibit nonzero onsite energies along with a two-scaled behavior of hoppings.

C. Comparison with older results for gapped AIM

In the literature, there are, in principle, two commonly known NRG-based proposals for solving gapped AIM problems. One relies on Wilson chains extrapolated from the corresponding AIM cases with $\Delta = 0$ [27,28,33]. In the other approach, standard NRG methods are used, but the gapped system is augmented with a weakly coupled metallic lead [21,22,26,31].

The main idea for the first approach centers around the extrapolation of the Wilson chain from the $\Delta = 0$ case by first employing the standard logarithmic discretization to the ungapped TDOS. For the gapped scenario, the Wilson chain is then terminated at M, so that the last hopping coefficient equals approximately Δ. The resulting tight-binding chain is then solved by the usual NRG iterative diagonalization. Using the unrescaled spectrum of eigenenergies at the last iteration in-gap state(s) are then identified directly.

Several problems, however, arise in such a construction. Taking any finite Δ, we note that the logarithmic discretization (as any other running up to the Fermi energy) inevitably crosses into the gap region at some given N and the Wilson chain should rigorously terminate here. However, the characteristic energy scale of the hopping here is only $\Lambda^{-N/2} \approx \sqrt{\Delta}$ and thus much larger than the desired one. Artificially, we then take $M = 2N + 1$ which thus protrudes into the undefined gap region of TDOS with $\Delta \neq 0$, but has the last hopping of order Δ. Closing of the gap thus requires employing an ever-growing Wilson chain of the $\Delta = 0$ AIM. The main issue of the method is thus not the strict finiteness of the employed Wilson chain but its generalization beyond the maximum allowed length of N.

On the other hand, the method with auxiliary metallic lead generates all Wilson chains using only standard NRG techniques, on the expense of adding a weakly coupled metallic lead to the system. So the original gap region is populated by a
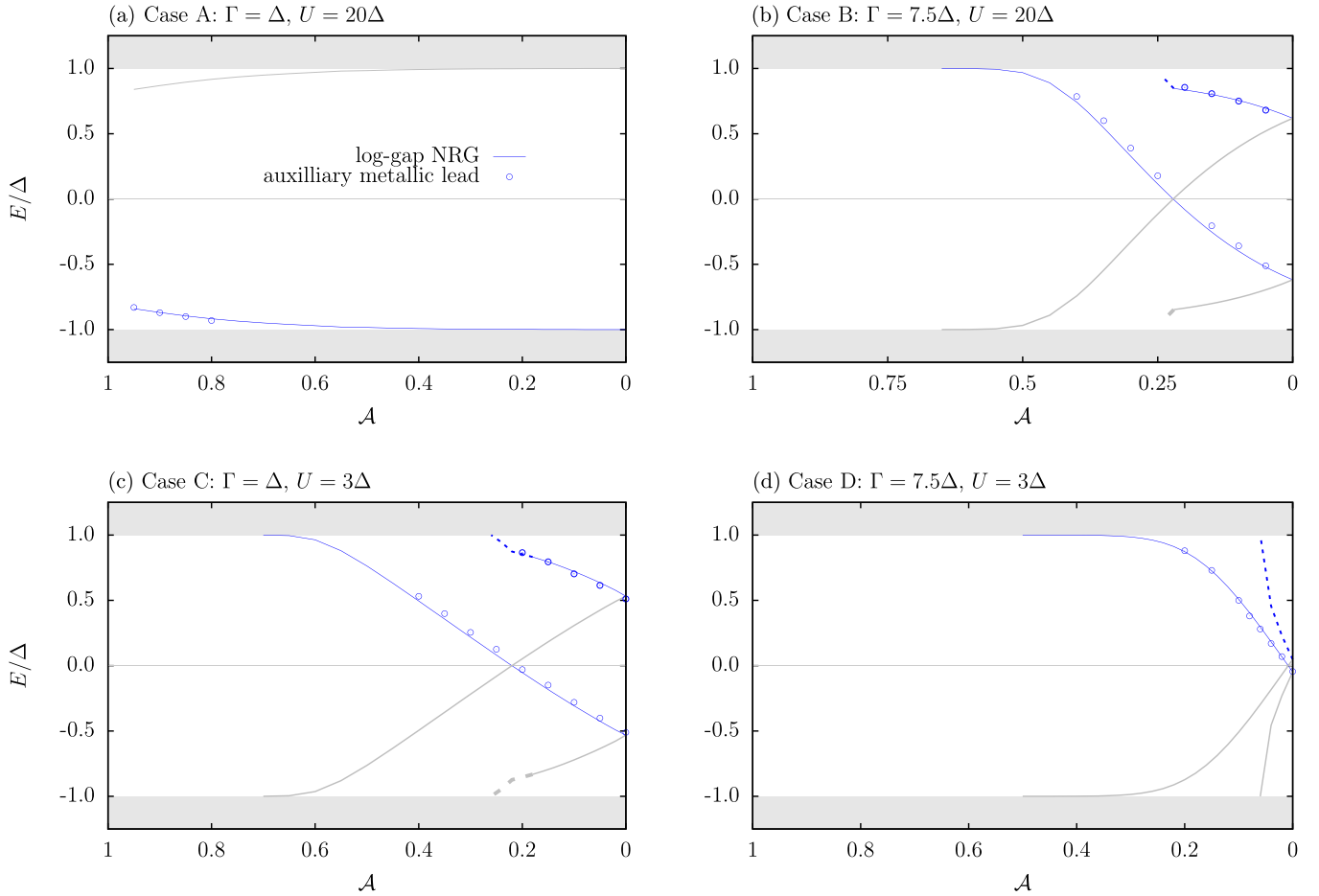
FIG. 7. (a)–(d) $\mathcal{A}$-dependent behavior of subgap excitations for four selected cases A, B, C, and D of the gapped AIM with constant TDOS according to Fig. 6 calculated with the log-gap NRG at $\Lambda = 2$. Solid and dashed lines represent one- and two-particle excitations, respectively. The solid thin gray lines show the result for the model with $\mathcal{A} \to -\mathcal{A}$. Results are compared with the NRG solution for the model augmented with auxiliary metallic lead (open circles), as performed in Ref. [22]. Due to the restrictions of the latter method only one-particle excitations could be determined. Using the one- and two-particle excitations, no in-gap states have been found to escape into the continuum, which is the main difference from the SC-AIM case shown in Fig. 5.

small but nonzero TDOS. To extract information about the gap region itself, a series of spectral functions at decreasing coupling Γ_M of the metallic lead are calculated. Subsequently, the gap region is scanned for the presence of subgap peaks, which are present as broadened analogs of the sharp in-gap peaks. The $\Gamma_M \to 0$ limit is then extrapolated from such a series, which is time consuming and inaccurate as a nonzero numeric threshold on the smallest possible Γ_M exists. Moreover, there is no guarantee for the $\Gamma_M = 0$ case to adiabatically connect to the series with supporting evidence being only circumstantial for the SC-AIM problem [21,31]. Additionally, this indirect method is not able to give indisputable conclusions about the quantum numbers of the GSs and in-gap states in question, nor can it be applied if the broadened in-gap peaks interfere with the gap edge or with the induced Kondo peak close to the Fermi energy. Taken together, both of the existing methods do not represent a rigorous Wilsonian RG approach to the fully gapped problem, and deviations from true solutions might be expected.

Let us therefore compare the log-gap NRG to the method of the auxiliary metallic lead by using the data from Fig. 7. Overall, the in-gap peak energies E_p are delivered in very

good quantitative agreement, with case B being the least accurate (large U/Δ and Γ/Δ). Systematic issues of the method with auxiliary metallic lead are well visible in all cases close to the gap edge and close to the Fermi energy due to the reasons discussed above. Additionally, the smallest

TABLE I. Energy of in-gap peaks E for AIM with constant but gapped TDOS wit $U = 4\Delta$, $\varepsilon_d = -U/2$, $\Gamma = 0.4\Delta$, $\mathcal{A} = 0$, and three values of Δ/B. Using the Haldane formula for the Kondo temperature, e.g., $T_K = \sqrt{U\Gamma/2}e^{\pi \varepsilon_d (\varepsilon_d + U)/(2U\Gamma)}$, cases A, B, C correspond to $T_K = 0.00176B$. Values taken from Ref. [28] have been compared to the log-gap method developed in this paper and to the method with auxiliary metallic lead adapted from Refs. [21,22,26,31].

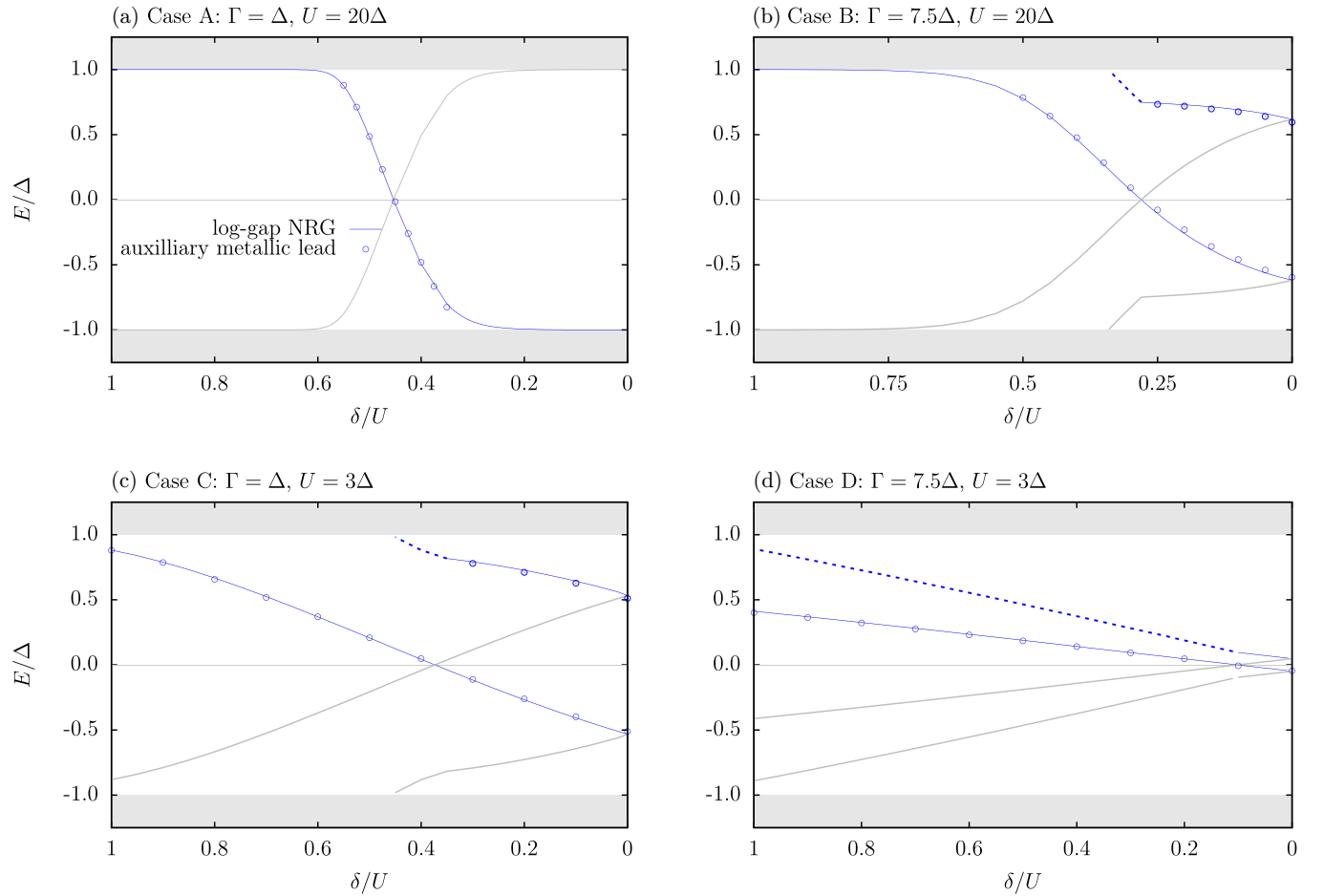|	Case	A	B	C
	Δ/T_k	0.004	0.065	0.800
	Δ/B	7.05×10^{-6}	1.15×10^{-4}	1.41×10^{-3}
Ref. [28]	$|E/B|$	1.76×10^{-7}	3.35×10^{-5}	1.23×10^{-3}
Auxiliary	$|E/B|$	8.29×10^{-8}	1.82×10^{-5}	1.02×10^{-3}
Log-gap	$|E/B|$	9.29×10^{-8}	2.15×10^{-5}	1.06×10^{-3}

FIG. 8. (a)–(d) δ-dependent behavior of subgap excitations for four selected cases A, B, C, and D of the gapped AIM with constant TDOS according to Fig. 6 calculated with the log-gap NRG at $\Lambda = 2$. Solid and dashed lines represent one- and two-particle excitations, respectively. The solid thin gray lines show the result for the model with $\mathcal{A} \to -\mathcal{A}$. Results are compared with the NRG solution for the model augmented with auxiliary metallic lead (open circles), as performed in Ref. [22]. Due to the restrictions of the latter method, only one-particle excitations could be determined.

value of numerically allowed Γ_M typically induces strong broadening of the in-gap peaks and reading off E is then associated with further systematic errors. Nevertheless, the obtained data points allow us to conclude that the log-gap NRG and the method of the auxiliary metallic lead agree very well and may be used interchangeably if required.

Let us finally assess the remaining method, where Wilson chains are extrapolated from the $\Delta = 0$ AIM. To this end, we first select the three cases discussed in Fig. 2 of Ref. [28] and then move to a more elaborate data set as presented in Fig. 3 therein. We thus read off the values of E from Fig. 2 in Ref. [28] and apply the remaining methods to recalculate the values with the corresponding model parameters as indicated in Ref. [28], e.g., $U = 4\Delta$, $\Gamma = 0.4\Delta$, $\mathcal{A} = 0$, and Δ/B varying. The resulting values of in-gap peak positions are shown in Table I and in Fig. 9. We stress that only the method with auxiliary metallic lead requires an explicit calculation of spectral functions as discussed in detail in the Appendix, while the other two rely directly on the unrescaled spectrum of NRG eigenvalues at the last iteration.

From Table I, the correspondence between the method of auxiliary metallic lead and the herein developed NRG

approach is once again confirmed to be good, with the two methods differing only by 20% the most. The difference is, however, to be attributed mostly to the difficulties with constructing the $\Gamma_M \to 0$ limit and is thus purely of numeric character. Contrary to this, the results from Ref. [28] differ up to almost 200% and are thus significantly deviating from the other methods. While the discrepancy seems to increase as $\Delta \to 0$, we systematically investigate the behavior of E when $\Delta \to 0$. Doing so, we closely follow the data set of Fig. 3 of Ref. [28] and set $\mathcal{A} = 0$ by using four different sets of U and Γ to match those in Ref. [28]. The values of T_K re assigned according to the Haldane formula $T_K = \sqrt{U\Gamma/2}e^{\pi\varepsilon_d(\varepsilon_d+U)/(2U\Gamma)}$ when $\Delta = 0$. We stress that the definition is inline with that stated explicitly in Ref. [28]. The results are presented in Fig. 9 as plots of E/Δ against Δ/T_K which then reveal universal scaling properties of the gapped AIM.

Qualitatively, we confirm that E is proportional to Δ^2/T_K as long as $\Delta/T_K < 10^{-2}$ which is demonstrated by the solid lines in Fig. 9. The same result is also stated in Ref. [28] and reproduced here by a dotted-dashed black line. Two additional data sets fot $T_K < 10^{-5}$ have been added to demonstrate
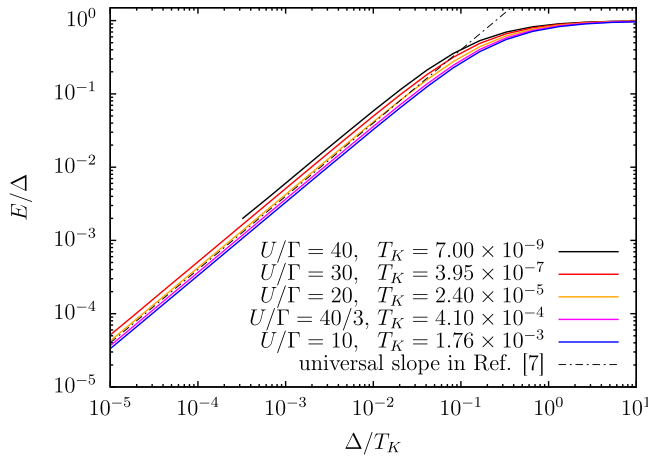
FIG. 9. The relative position of in-gap peaks in the gap, e.g., E/Δ demonstrates universal linear behavior with Δ/T_K over a broad range. Here, T_K is determined according to the Haldane formula, when $\Delta = 0$. Five different ratios Γ/U are plotted to document the substantial vertical offset that accompanies the linear regime, a behavior not observed in Ref. [28]. Three largest values of T_K correspond to those investigated therein.

the sensitivity of the log-gap NRG method, even to fine details. Consequently, two major problems with the results in Ref. [28] became visible. First, upon closer inspection, it is evident that the actual computed values of E oscillate around the linear dependence which was thus probably fitted to the data. Even more importantly, the log-gap NRG results show vertical offsets that are T_K dependent, an effect not detected at all in Ref. [28]. While the offsets appear relatively modest, one has to take into account the logarithmic nature of the plots.

Consequently, differences in E for $T_K = 2.4 \times 10^{-5}$ are almost negligible between both methods, but already for $T_K = 1.76 \times 10^{-3}$ the offset generates $\approx 25\%$ of the difference in the linear regime. Interestingly, in case A from Table I the difference was even much larger of almost 100%, which is an additional effect of the oscillatory deviations from the predicted line, as these are severe enough to increase the error significantly. None of these problems arise in the log-gap NRG approach, and a very broad range of parameters can be evaluated since only the $T_K = 7 \times 10^{-9}$ curve becomes numerically instable below $\Delta/T_K < 4 \times 10^{-4}$.

Given the methodological problems, when Wilson chains are extrapolated from $\Delta = 0$, the observed differences to the remaining two methods, which use rigorous NRG techniques, is to be expected. We can thus safely conclude that the generalized Wilson chains according to Refs. [27,28,33] are not completely representing the actual AIM with constant but gapped TDOS, but can capture many qualitative aspects of the present system correctly.

VI. CONCLUSIONS

We have reported on a NRG scheme that lifts the so far existing limits on solving impurity problems immersed in scalar but gapped TDOS via unbiased Wilsonian RG techniques. The herein developed method is referred to as the log-gap

NRG approach since it replaces the standard logarithmic discretization that runs up to the Fermi energy with an analogous procedure that accumulates the discretization points logarithmically at the gap edges. While the subsequent tridiagonalization is standard, the resulting Wilson chains contain generally two scalings that require specific diagonalization procedure, where truncation of the Hilbert space is performed only at every even NRG iteration (initial iteration enumerated as 0th).

Both the log-gap discretization and the alternating kept or discarded scheme for truncation of the Hilbert space during the iterative solution of the Wilson chain are inherently connected. The discretization procedure is motivated by the analysis of the poles in the discretized tunneling self-energy in Sec. III B and gives rise to two-scaled behavior of the Wilson chain, which requires different truncation strategy of the resulting Hilbert space so that the energy scale separation is not broken. The two-scaled nature of SC-AIM and the gapped AIM hint towards the underlying RG universality class.

Using the NRG technique, first a thorough benchmarking was performed using SC-AIM in its scalar representation, as obtained in Ref. [31]. The results by the log-gap NRG approach compare in high numeric accord to standard NRG methods, but we stress that the log-gap NRG approach is superior in terms of CPU requirements due to the available symmetries. This holds true also when $\varepsilon_d \neq -U/2$ or nonzero magnetic field on the QD is considered. The generalization to encompass such cases is straightforward and of interest for current experiments where the log-gap NRG method can provide much faster scanning tool in the parameter space of SC-AIM (especially when its approximate version from Appendix A is employed).

The log-gap NRG approach was then finally used in the unbiased Wilsonian RG solution of the AIM with constant but gapped TDOS. The resulting physical quantities are thus valid without any restrictions at arbitrary temperatures corresponding to the given length of the chain. The most general conclusion from these calculations is that the model behaves qualitatively as SC-AIM as they both belong to the same RG equivalence class. In particular, one observes always a doublet GS in a completely particle-hole symmetric scenario with $\mathcal{A} = 0$ and $\varepsilon_d = -U/2$, which corresponds to the $\varphi = \pi$ scenario of SC-AIM. Nevertheless, dependent on the values of Γ and U it may eventually undergo a QPT into a singlet GS as $\mathcal{A}$ is increased, which corresponds to decreasing φ in SC-AIM. A complete phase diagram in a half-filled QD scenario is shown in Fig. 6, which is highly similar to the corresponding phase diagram of SC-AIM calculated in Fig. 4. When the QD is away from half-filling but $\mathcal{A} = 0$, the problem simplifies greatly as the resulting Wilson chain contains only the usual scaling of hoppings and all onsite energies are zero. Nevertheless, the RG flow and the resulting subgap spectroscopy, as performed in Fig. 8, are similar to that of a particle-hole asymmetric band.

In Sec. V C, an elaborate comparison has been performed that shows that the existing results from Refs. [27,28,33] are not only in conflict with the here developed log-gap NRG method, but, crucially, they show also significant numeric discrepancy when compared to the standard NRG method for a system augmented with an auxiliary metallic lead. Contrary
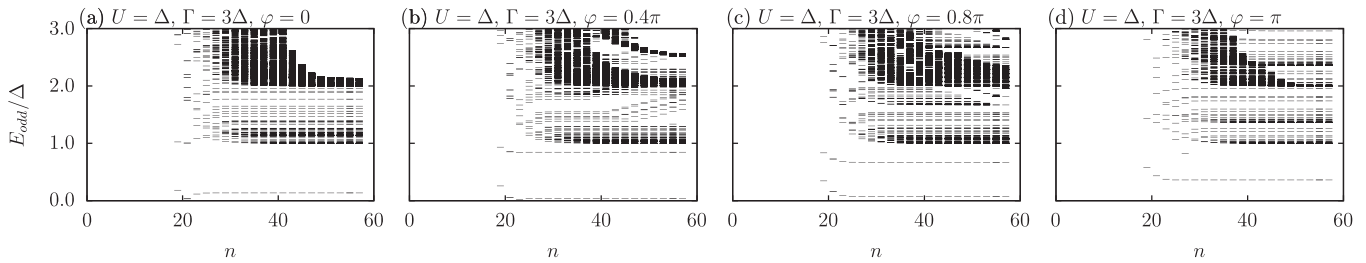
FIG. 10. (a)–(d) φ-dependent behavior of NRG eigenspectra when the Wilson chains of SC-AIM with corresponding parameters obtained by the log-gap discretization are subject to the usual iterative diagonalization in which states are discarded at every iteration. Obviously, $\varphi = 0$ and π cases do not suffer from corruption, but for all other choices, states in the middle of the supragap spectrum experience unphysical flow, which is only a numeric artifact.

to this, the herein developed log-gap NRG matches very well such results, as documented in Figs. 7 and 8. Additional reasons for the approach of Refs. [27,28,33] to be considered with caution is of theoretic origin and were presented also in Sec. V C.

We stress that the method is general and not restricted to SC-AIM or AIM with constant but gapped TDOS. Future generalizations and developments can incorporate the

z-averaging techniques to solve for the spectral function, while the addition of an out-of-half-filling scenario or the presence of magnetic field is almost trivial. Additionally, an asymmetrically placed gap around the Fermi energy, as can appear in realistic TDOS functions [41], can also easily be incorporated. Another natural avenue for important applications of the here presented method represents the problem of metal-insulator transition, where the herein proposed NRG
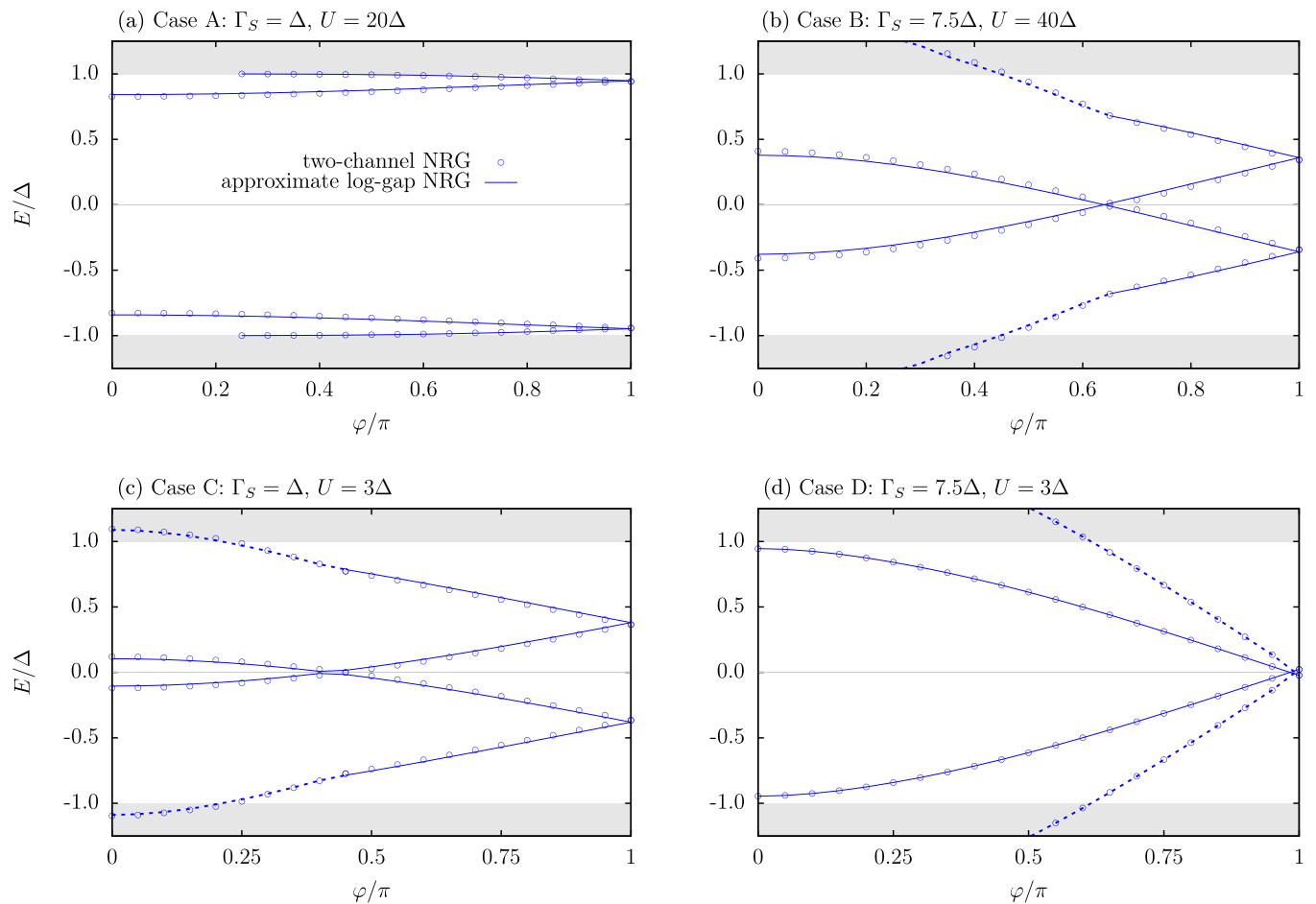

FIG. 11. (a)–(d) φ-dependent behavior of in-gap states for four selected cases A, B, C, and D of SC-AIM according to Fig. 4 obtained using log-gap discretization with usual Wilson chain diagonalization procedure, where states are (eventually) discarded after every iteration. While the eigenspectra are generally corrupted, as shown in Fig. 10, the subgap portion is altered only marginally and can be used for quick scans for QPTs. We stress, however, that thermodynamic quantities or spectral functions would suffer from systematic errors, and this approximate approach should be discouraged in such instances.

scheme might be implemented as internal impurity solver in DMFT calculations when the gap is finally open in the system. However, precaution is always required as the presence of the second-stage scaling is a necessary prerequisite for meaningful application of RG techniques. Moreover, some additional problems might arise when the gap edge is not sharply defined, as already noted in [22]. For realistic scenarios, fusion with the adaptive mesh approach according to [42] is also necessary.

As a final consequence of the presented approach, we would like to accentuate the missing rigorous RG theory of an effective model for SC-AIM. While zero bandwidth or atomic limit theory are nowadays routinely employed for qualitative analysis of SC-AIM and related experiments [25,43–45], we are still not able to fully understand how and why they emerge from the full problem. The two-scaled nature of the Wilson chains, as deciphered here, could however allow to build a rigorous analytic RG theory of fixed points in the spirit of seminal works by Wilson [10–12].

Taking all this together, one of the main limitations of the NRG approach has been successfully eliminated, so an unbiased Wilsonian RG approach for gapped systems is now able to resolve all energy scales at the same footing. Further generalization and development is, however, necessary to go beyond the basic models implemented here.

ACKNOWLEDGMENTS

APPENDIX A: APPROXIMATE VERSION OF THE LOG-GAP NRG APPROACH

In the main text, only the results of a rigorous Wilsonian RG approach are used. However, as briefly mentioned in Sec. IV, an approximate and much faster calculation (in terms of the used CPU time) can be used for either preliminary scanning of large parametric spaces or for obtaining subgap properties with relatively small numerical deviations from the actual ones, as demonstrated here.

The main idea is to use the ordinary kept or discarded strategy as outlined in Fig. 3 in conjunction with the log-gap discretization. States are thus discarded after each iteration, and the energy scale separation is inevitably broken. Consequently, the eigenenergy spectra are corrupted especially in the high-energy sector, as shown in Fig. 10 for SC-AIM with $\varepsilon_d = -U/2, U = 3\Delta$, and $\Gamma = \Delta$. Notably, $\varphi = 0$ and $\varphi = \pi$ remain exact.

In Fig. 11, we then demonstrate that the subgap portion of eigenenergies is nevertheless well usable, at least in an approximate manner, with a relative error of the order of just few percent when compared to the standard two-channel NRG. We stress, however, that such calculations might be dangerous without any reference data from exact Wilsonian approaches. Moreover, they should never be used for obtaining spectral functions due to the corruption of the high-energy spectrum.
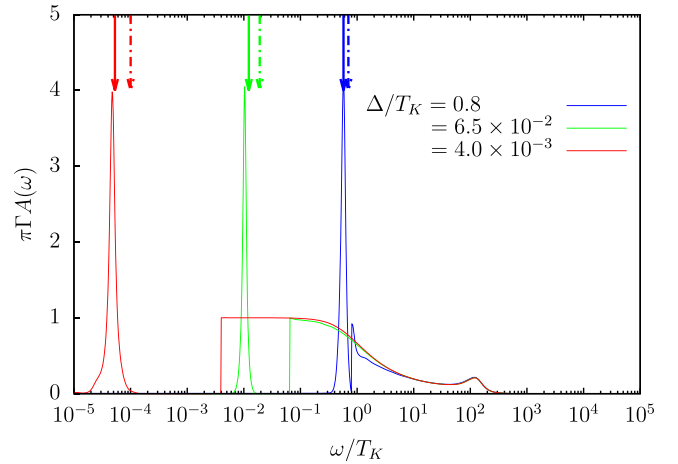

FIG. 12. Solid lines show spectral functions calculated with the auxiliary metallic lead according to Refs. [21,22,26,31]. Solid arrow shows the position of the in-gap peaks calculated using the log-gap approach, while dashed arrows are placed in positions corresponding to Fig. 3 of Ref. [28]. Note the overall good equivalence between the log-gap and auxiliary metallic lead methods, while values using the approach of Refs. [27,28] are clearly misaligned with the other two results. Parameters for the AIM with constant but gapped TDOS are $U = 4B$, $\Gamma = 0.4B$, $\mathcal{A} = 0$, and Δ/B varying according to the legend.

APPENDIX B: SPECTRAL FUNCTIONS IN THE METHOD OF AUXILIARY METALLIC LEAD

Using the method of auxiliary metallic lead, the presence of the subgap levels cannot be directly inferred from the (un)rescaled spectrum of eigenenergies due to the presence of the metallic lead [21,22,26,31]. Instead, spectral functions are obtained and analyzed. In this respect, we note that the added metallic lead populates the total TDOS in the gap region with small but nonzero values and eliminates thus any need of separation of the collected delta peaks into subgap or supragap ones as required in the method of Refs. [27,28]. In the end, throughout the DM-NRG run, one collects a multitude of delta peaks appear inside of the gap region. While most of these have small spectral weights and form just a small but nonzero background in the gap region, there is always an ensemble of delta peaks centered around specific frequencies that contain a significant total spectral weight and give rise to the in-gap spectral peaks as those shown in Fig. 12. Their finite spectral weight upon decreasing Γ_M, the coupling of the metallic lead to the system, to 0 has been demonstrated in Ref. [22] for various TDOS functions. In other words, no single isolated delta peak, but rather a collection of delta peaks, comprises the few distinct peaks in the obtained spectral function. The resulting broadening of the in-gap spectral features results thus primarily from the added metallic lead and not from the selected broadening procedure.

In Fig. 12, corresponding to Table I, we note that closing the gap at fixed U and Γ causes the in-gap states to rapidly approach the Fermi energy, where a Kondo peak develops due to the auxiliary metallic lead. The accurate reading of the in-gap peak position becomes, therefore, increasingly

complicated. Nevertheless, such a problem arises mainly for the case of $\Delta = 7.05 \times 10^{-6}B$, while all in-gap positions determined in Ref. [28] are systematically larger than with the auxiliary lead by a factor of up to 2. Let us also stress that the supragap portion of the spectral function sharply drops at the gap edge, as expected. Contrary, in Fig. 2 of Ref. [28] one observes a spillover of the supragap spectral functions into the gap region. We thus conclude that the method used in Ref. [28] is highly approximate and inconsistent even on its own. Contrary to this, in Ref. [22] in-gap peaks at $\mathcal{A} = 0$ have always appeared inside of a well-defined gap which is also confirmed after recalculating the three cases of Ref. [28].

APPENDIX C: TECHNICAL DETAILS OF NRG IMPLEMENTATIONS

In the presented work, all model parameters are measured in units of B, where $2B$ is the width of the band. A typical value of the gap for SC-AIM as well as the gapped AIM with constant TDOS is set to $0.0005B$ if not stated otherwise. The effects of finite bandwidth are thus essentially almost completely suppressed. Two standard NRG calculations have been implemented within the open source code of NRG LJUBLJANA [46]: the standard two-channel NRG for SC-AIM

[38] and the one-channel calculation for systems augmented with metallic leads as described in Refs. [26,31]. The former has been performed at $\Lambda = 4$ while for the latter $\Lambda = 2$ due to the one-channel nature of the calculation. In both cases, at least 1000 states have been kept.

The here-developed log-gap NRG algorithm has been implemented in the flexible DM-NRG BUDAPEST code [47] by modifying its kept or discarded routines. Log-gap discretization (29) was performed in a *Mathematica* script with a subsequent tridiagonalization performed in a standalone $C++$ code. The resulting Wilson chain parameters were then manually fed into the DM-NRG BUDAPEST code. After the discarding step of the diagonalization scheme (see Sec. IV), 500 multiplets have been kept, which have been tested to be sufficient to have no impact on the subgap properties of the presented results. $\Lambda = 2$ was set due to the one-channel nature of the Wilson chain.

To make the general idea of the log-gap NRG method more transparent and to streamline the presentation, the z averaging was not employed. More specifically, the in-gap positions have been calculated at single value of $z = 1$. This applies to the log-gap NRG approach introduced in this paper as well as to all standard NRG calculations performed within NRG LJUBLJANA with the exception of supragap function shown in Fig. 9.

[1] P. W. Anderson, Phys. Rev. **124**, 41 (1961).

[2] P. A. Lee, T. M. Rice, J. W. Serene, L. J. Sham, and J. W. Wilkins Condens. Matter Phys. **12**, 99 (1986).

[3] A. C. Hewson, *The Kondo Problem to Heavy Fermions*, Cambridge Studies in Magnetism (Cambridge University Press, Cambridge, 1993).

[4] T. A. Fulton and G. J. Dolan, Phys. Rev. Lett. **59**, 109 (1987).

[5] S. M. Cronenwett, T. H. Oosterkamp, and L. P. Kouwenhoven, Science **281**, 540 (1998).

[6] M. Pustilnik and L. Glazman, J. Phys.: Condens. Matter **16**, R513 (2004).

[7] A. K. Mitchell, K. G. L. Pedersen, P. Hedegård, and J. Paaske, Nat. Commun. **8**, 15210 (2017).

[8] V. Madhavan, W. Chen, T. Jamneala, M. F. Crommie, and N. S. Wingreen, Science **280**, 567 (1998).

[9] J. Li, W.-D. Schneider, R. Berndt, and B. Delley, Phys. Rev. Lett. **80**, 2893 (1998).

[10] K. G. Wilson, Rev. Mod. Phys. **47**, 773 (1975).

[11] H. R. Krishna-murthy, J. W. Wilkins, and K. G. Wilson, Phys. Rev. B **21**, 1003 (1980).

[12] H. R. Krishna-murthy, J. W. Wilkins, and K. G. Wilson, Phys. Rev. B **21**, 1044 (1980).

[13] P. Kopietz, L. Bartosch, and F. Schütz, *Introduction to the Functional Renormalization Group*, Lecture Notes in Physics (Springer, Berlin, 2010).

[14] S. Streib, A. Isidori, and P. Kopietz, Phys. Rev. B **87**, 201107(R) (2013).

[15] A. C. Hewson, Phys. Rev. Lett. **70**, 4007 (1993).

[16] V. Janiš and P. Augustinský, Phys. Rev. B **75**, 165108 (2007).

[17] V. Janiš, P. Zalom, V. Pokorný, and A. Klíč, Phys. Rev. B **100**, 195114 (2019).

[18] K. Takegahara, Y. Shimizu, and O. Sakai, J. Phys. Soc. Jpn. **61**, 3443 (1992).

[19] E. Gull, A. J. Millis, A. I. Lichtenstein, A. N. Rubtsov, M. Troyer, and P. Werner, Rev. Mod. Phys. **83**, 349 (2011).

[20] J. E. Gubernatis, *Quantum Monte Carlo Methods: Algorithms for Lattice Models* (Cambridge University Press, New York, 2016).

[21] P. Zalom and T. Novotný, Phys. Rev. B **104**, 035437 (2021).

[22] P. Zalom and M. Žonda, Phys. Rev. B **105**, 205412 (2022).

[23] T. Hecht, A. Weichselbaum, J. von Delft, and R. Bulla, J. Phys.: Condens. Matter **20**, 275213 (2008).

[24] B. W. Heinrich, J. I. Pascual, and K. J. Franke, Prog. Surf. Sci. **93**, 1 (2018).

[25] V. Meden, J. Phys.: Condens. Matter **31**, 163001 (2019).

[26] G. Diniz, G. S. Diniz, G. B. Martins, and E. Vernek, Phys. Rev. B **101**, 125115 (2020).

[27] K. Chen and C. Jayaprakash, Phys. Rev. B **57**, 5225 (1998).

[28] C. P. Moca and A. Roman, Phys. Rev. B **81**, 235106 (2010).

[29] M. R. Galpin and D. E. Logan, Phys. Rev. B **77**, 195108 (2008).

[30] C. P. Moca, I. Weymann, M. A. Werner, and G. Zaránd, Phys. Rev. Lett. **127**, 186804 (2021).

[31] P. Zalom, V. Pokorný, and T. Novotný, Phys. Rev. B **103**, 035419 (2021).

[32] R. Žitko, D. Hansen, E. Perepelitsky, J. Mravlje, A. Georges, and B. S. Shastry, Phys. Rev. B **88**, 235132 (2013).

[33] J. Pinto and H. Frota, J. Magn. Magn. Mater. **379**, 217 (2015).

[34] A. Kadlecová, M. Žonda, and T. Novotný, Phys. Rev. B **95**, 195114 (2017).

[35] R. Bulla, J. Keller, and T. Pruschke, Z. Phys. B: Condens. Matter **94**, 195 (1994).

[36] R. Bulla, T. A. Costi, and T. Pruschke, Rev. Mod. Phys. **80**, 395 (2008).

[37] J.-G. Liu, D. Wang, and Q.-H. Wang, Phys. Rev. B **93**, 035102 (2016).

[38] K. Satori, H. Shiba, O. Sakai, and Y. Shimizu, J. Phys. Soc. Jpn. **61**, 3239 (1992).

[39] L. Pavešič, R. Aguado, and R. Žitko, arXiv:2304.12456.

[40] V. Pokorný and M. Žonda, Phys. Rev. B **107**, 155111 (2023).

[41] P. A. Almeida, M. A. Manya, M. S. Figueira, S. E. Ulloa, E. V. Anda, and G. B. Martins, arXiv:2305.18121.

[42] R. Žitko, Comput. Phys. Commun. **180**, 1271 (2009).

[43] T. Meng, S. Florens, and P. Simon, Phys. Rev. B **79**, 224521 (2009).

[44] K. Grove-Rasmussen, G. Steffensen, A. Jellinggaard, M. H. Madsen, R. Žitko, J. Paaske, and J. Nygård, Nat. Commun. **9**, 2376 (2018).

[45] M. Žonda, P. Zalom, T. Novotný, G. Loukeris, J. Bätge, and V. Pokorný, Phys. Rev. B **107**, 115407 (2023).

[46] R. Žitko, NRG LJUBLJANA (8f90ac4), Zenodo, https://doi.org/10.5281/zenodo.4841076.

[47] A. I. Tóth, C. P. Moca, O. Legeza, and G. Zaránd, Phys. Rev. B **78**, 245109 (2008).